EURASIP Journal on Advances in Signal Processing
a SpringerOpen Journal

RESEARCH Open Access

Remotely-sensed TOA interpretation of synthetic UWB based on neural networks

Hao Zhang[1,3*], Xue-rong Cui[1,2] and T Aaron Gulliver[3]

Abstract

Because of the good penetration into many common materials and inherent fine resolution, Ultra-Wideband (UWB) signals are widely used in remote sensing applications. Typically, accurate Time of Arrival (TOA) estimation of the UWB signals is very important. In order to improve the precision of the TOA estimation, a new threshold selection algorithm using Artificial Neural Networks (ANN) is proposed which is based on a joint metric of the skewness and maximum slope after Energy Detection (ED). The best threshold based on the signal-to-noise ratio (SNR) is investigated and the effects of the integration period and channel model are examined. Simulation results are presented which show that for the IEEE802.15.4a channel models CM1 and CM2, the proposed ANN algorithm provides better precision and robustness in both high and low SNR environments than other ED-based algorithms.

Keywords: Artificial Neural Network (ANN), Remote sensing, Ultra-Wideband (UWB), TOA estimation, Ranging, Skewness

Introduction

As a new wireless communications technology, Ultra-Wideband (UWB) has generated considerable research interest due to the many potential applications. One of the most promising areas is remote sensing [1,2]. For example, Defense Research and Development Canada (DRDC) Ottawa has conducted numerous experiments on indoor through-wall imaging, snow penetration, stand-off remote sensing of human subjects, and mine detection using high-resolution UWB signals [1]. In [2], UWB propagation channel characterization was performed to test the feasibility of using UWB technology in underground mining to monitor and communicate with remote sensors.

UWB technology offers many advantages for remote sensing [1]. First, some frequency components may be able to penetrate obstacles to provide a Line-Of-Sight (LOS) signal. Second, the transmission of very short pulses makes high time resolution (sub-nanosecond to nanosecond) possible. Third, the wide signal bandwidth means a very low power spectral density, which reduces interference to other Radio Frequency systems.

Among the potential applications, precision ranging or Time of Arrival (TOA) estimation is the most important for remote sensing. However, this is a very challenging problem due to the severe environments encountered, e.g., thermal noise, multi-path fading, reflection interference, and inter-symbol interference. The TOA estimation problem has extensively been studied [3-6]. There are two approaches applicable to UWB technology, a Matched Filter (MF) [3] (such as a Rake or correlation receiver) with a high sampling rate and high-precision correlation, or an Energy Detector (ED) [4-6] with a lower sampling rate and low complexity. An MF is the optimal technique for TOA estimation, where a correlator template is matched exactly to the received signal. However, an UWB receiver operating at the Nyquist sampling rate makes it very difficult to align with the multipath components of the received signal [7]. In addition, an MF requires *a priori* estimation of the channel, including the timing, amplitude, and phase of each multipath component of the impulse [7]. Because of the high sampling rates and channel estimation, an MF may not be practical in many applications. As opposed to a more complex MF, an ED is a non-coherent approach to TOA estimation. It consists of a square-law device,

* Correspondence: zhanghao@ouc.edu.cn
[1]Department of Information Science and Engineering, Ocean University of China, Qing Dao, China
[3]Department of Electrical Computer Engineering, University of Victoria, Victoria, Canada
Full list of author information is available at the end of the article

followed by an integrator, sampler, and a decision mechanism. The TOA estimate is made by comparing the integrator output with a threshold and choosing the first sample to exceed the threshold. It is a practical solution as it directly yields an estimate of the start of the received signal. An ED is thus a low complexity, low sampling rate receiver that can be employed without the need for *a priori* channel estimation.

The major challenge with ED is the selection of an appropriate threshold based on the received signal samples. Threshold selection for different signal-to-noise ratios (SNRs) has been investigated via simulation. In [4], a normalized threshold selection technique for TOA estimation of UWB signals was proposed which uses exponential and linear curve fitting of the kurtosis of the received samples. In [5], an approach based on the minimum and maximum sample energy was introduced. These approaches have limited TOA precision, as the strongest path is not necessarily the first arriving path.

Neural networks (NNs) have extensively been used in signal processing applications. The weights between the input and output layers can be adjusted to minimize the error between the input and output. Because of the complexity of wireless environments, it is difficult to derive a closed-form expression to estimate the TOA. On the other hand, an artificial neural network (ANN) can provide a very flexible mapping based on the training input. The ANN here intends to solve a regression problem being J the input and optimal threshold the output.

In this article, we consider the relationship between the SNR and the statistics of the integrator output including skewness, maximum slope, kurtosis and standard deviation. A metric based on skewness and maximum slope is then used as the ANN input. A back propagation (BP) NN is used which is a feed forward NN. It approximates the relationship between the joint metric and the optimal threshold by using a nonlinear continuum rational function. Performance results are presented which show that in the IEEE 802.15.4a channel models CM1 and CM2, this ANN provides robust estimates with high precision for both high and low SNRs.

The remainder of this article is organized as follows. In the following section, the system model is presented. Section "TOA estimation based on ED" discusses TOA estimation algorithms based on ED. Section "Statistical characteristics of the signal energy" considers the statistical characteristics of the energy values, and a joint metric based on skewness and maximum slope is proposed. In Section "Optimal normalized threshold with respect to J", the relationship between the joint metric and optimal normalized threshold is established. Section "Threshold selection using an ANN based on skewness and maximum slope" introduces a novel TOA estimation algorithm based on an ANN. Some performance results are presented in Section "Performance results and discussion", and Section "Conclusions" concludes the article.

System model

IEEE 802.15.4a [8] is the first international standard that specifies a wireless physical layer to enable precise TOA estimation and wireless ranging. It includes channel models for indoor residential, indoor office, industrial, outdoor, and open outdoor environments, usually with a distinction between LOS and non-LOS (NLOS) properties. In this article, a Pulse Position Modulation Time Hopping UWB (PPM-TH-UWB) signal [9] is employed for transmission between the transmitter and receiver.

UWB signal

PPM-TH-UWB signals are very short in time, typically a few nanoseconds, and can be expressed as

$$s(t) = \sum_{-\infty}^{+\infty} p\left(t - iT_f - c_i T_c - a_i \epsilon\right) \tag{1}$$

where i and T_f are the frame index and frame duration, respectively. The time hopping TH is provided by a pseudorandom integer-valued sequence c_i, which differs for each user to allow for multiple access communications. T_c is the chip time, and the PPM time shift is ϵ, with the data a_i either 0 or 1. If a_i =1, the signal is shifted in time, otherwise there is no PPM shift. The pulse is given by $p(t)$. For example, the second derivative Gaussian pulse is given by

$$p(t) = \frac{d^2 f(t)}{dt^2} = \left(1 - 4\pi \frac{t^2}{\alpha^2}\right) e^{\frac{2\pi t^2}{\alpha^2}} \tag{2}$$

where α is the shape factor and $f(t)$ is the Gaussian pulse. A smaller value of α results in a shorter pulse duration and thus a larger bandwidth.

Multipath fading channel

Because of the multipath channel between the transmitter and receiver, the received signal can be expressed as

$$r(t) = \sum_{n=1}^{N} \alpha_n p(t - \tau_n) + n(t) \tag{3}$$

where N is the number of received multipath components, α_n and τ_n denote the amplitude and delay of the nth path, respectively, and $n(t)$ is additive white

Gaussian noise with zero mean and two-sided power spectral density $N_0/2$. Equation (3) can be rewritten as

$$r(t) = s(t) * h(t) + n(t) \tag{4}$$

where $s(t)$ is the transmitted signal, and $h(t)$ is the channel impulse response given by

$$h(t) = X\sum_{n=1}^{N_c}\sum_{n=1}^{K(n)}\alpha_{nk}\delta(t - T_n - \tau_{nk}) \tag{5}$$

where X is a log-normal random variable representing the amplitude gain of the channel, N_c is the number of observed clusters, $K(n)$ is the number of multipath components received within the nth cluster, α_{nk} is the coefficient of the kth component of the nth cluster, T_n is the TOA of the nth cluster and τ_{nk} is the delay of the kth component within the nth cluster.

Energy detector

As shown in Figure 1, after the Low Noise Amplifier, the received signal is squared, and then input to an integrator with integration period T_b. Because of the inter-frame leakage due to multipath signals, the integration duration is set to $3T_f/2$ [4], so the number of signal values for ED is $N_b = (3T_f)/(2T_b)$. The integrator output can then be expressed as

$$z[n] = \sum_{j=1}^{N_s}\int_{(j-1)T_f+(c_j+n)T_b}^{(j-1)T_f+(c_j+n-1)T_b} r^2(t)dt \tag{6}$$

where $n = 1, 2, \ldots, N_b$ is the sample index with respect to the start of the integration period and N_s is the number of pulses per symbol. Here, N_s is set to 1, so the integrator output is

$$z[n] = \int_{(c+n-1)T_b}^{(c+n)T_b} r^2(t)dt \tag{7}$$

If $z[n]$ is the integration of noise only, it has a centralized Chi-square distribution, while it has a non-centralized Chi-square distribution if a signal is present. The mean and variance of the noise and signal values are given by [4]

$$m_0 = Fs^2, s_0{}^2 = 2Fs^4, \tag{8}$$

$$m_e = Fs^2 + E_n, s_e{}^2 = 2Fs^4 + 4s^2E_n \tag{9}$$

respectively, where E_n is the signal energy within the nth integration period and F is the number of degrees of freedom given by $F = 2BT_b + 1$. B is the signal bandwidth.

TOA estimation based on ED

TOA estimation algorithms

There are many TOA estimation algorithms based on ED which can be used to determine the start of a received signal, as shown in Figure 2. The simplest one is Maximum Energy Selection (MES), which chooses the maximum energy value to be the start of the signal. The TOA is estimated as the center of the corresponding integration period

$$\tau_{MES} = \left[\underset{1\le n\le N_b}{\arg\max}\{z[n]\} - 0.5\right]T_b \tag{10}$$

However, as shown in Figure 2, the maximum energy value is not always the first [3], especially in NLOS environments. Often the first energy value $z[\hat{n}]$ is located before the maximum $z[n_{\max}]$, i.e., $\hat{n} \le n_{\max}$. Thus, Threshold Crossing (TC) TOA estimation has been proposed where the received energy values are compared to an appropriate threshold ξ. In this case, the TOA estimate is given by

$$\tau_{TC} = [\underset{1\le n\le n_{\max}}{\arg\min}\{n|z[n] >= \xi\} - 0.5]T_b \tag{11}$$

It is difficult to determine an appropriate threshold ξ directly, so a normalized threshold ξ_{norm} is usually employed with

$$\xi = \xi_{\text{norm}}(\max(z(n)) - \min(z(n))) + \min(z(n)) \tag{12}$$

The TOA estimate is then obtained using Equation (11). The problem in this case becomes one of how to set the threshold, i.e., how to establish the relationship between the received energy values and ξ_{norm}. There are two main methods in the literature, curve fitting and fixed threshold (FT). In [4], a normalized threshold selection technique for TOA estimation of UWB signals was proposed which uses exponential and linear curve fitting of the kurtosis of the received samples. A simpler approach is the FT algorithm where the threshold is set to a fixed value, for example $\xi_{\text{norm}} = 0.4$. If ξ_{norm} is set to 1, the algorithm is the same as MES. In this article, an ANN algorithm is employed to obtain the normalized threshold based on the signal energy statistics.

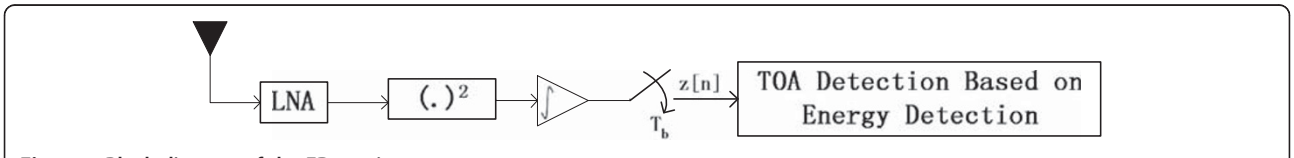

Figure 1 Block diagram of the ED receiver.

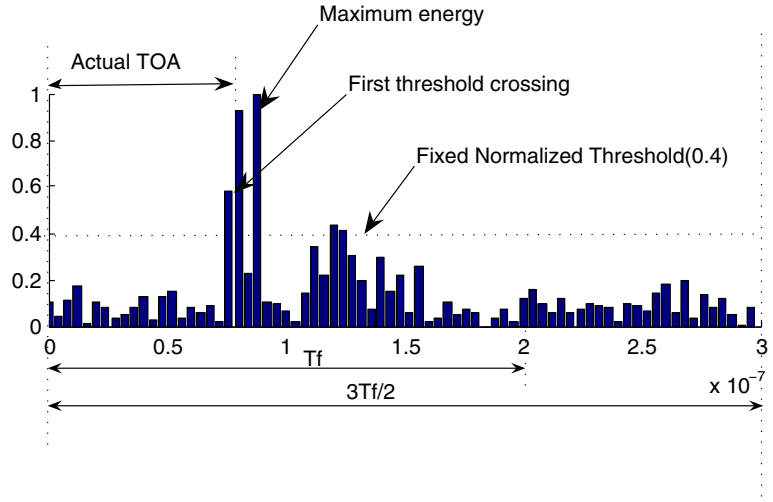

Figure 2 TOA estimation techniques based on received energy.

TOA estimation error

In [5], the mean absolute error (MAE) of TC-based TOA estimation was analyzed, and closed form error expressions derived. The MAE can be used to evaluate the quality of an algorithm, and is defined as

$$MAE = \frac{1}{N}\sum_{n=1}^{N}\left|t_n - \hat{t}_n\right| \tag{13}$$

where t_n is the nth actual propagation time,$\hat{t}_n$ is the nth TOA estimate, and N is the number of TOA estimates.

Statistical characteristics of the signal energy

In this section, the skewness**,** maximum slope, kurtosis and standard deviation of the energy values are analyzed.

Kurtosis

The kurtosis is calculated using the second- and fourth-order moments and is given by

$$k = \frac{1}{(N_b-1)\sigma^4}\sum_{i=1}^{N_b}(x_i-\bar{x})^4 \tag{14}$$

where $\bar{x}$ is the mean, and σ is the standard deviation. The kurtosis for a standard normal distribution is three. For this reason, k is often redefined as $K = k - 3$ (referred to as excess kurtosis), so that the standard normal distribution has a kurtosis of zero. Positive kurtosis indicates a "peaked" distribution, while negative kurtosis indicates a "flat" distribution. For noise only (or for a low SNR) and sufficiently large F (degrees of freedom of the Chi-square distribution), z[n] has a Gaussian distribution and $K = 0$. On the other hand, as the SNR increases, K tends to increase.

In [4], the normalized threshold with respect to the kurtosis and the corresponding MAE were investigated. To model this relationship, a double exponential function was used for T_b = 4 ns, and a linear function for T_b=1 ns with K as the x-coordinate and ξ_{best} as the y-coordinate. The resulting expressions are

$$\xi_{best}^{(4ns)} = 0.673e^{-0.75\log_2 K} + 0.154e^{-0.001\log_2 K} \tag{15}$$

and

$$\xi_{best}^{(1ns)} = -0.082\log_2 K + 0.77 \tag{16}$$

The model coefficients were obtained using data from both the CM1 and CM2 channels.

Skewness

The skewness is given by

$$S = \frac{1}{(N_b-1)\sigma^3}\sum_{i=1}^{N_b}(x_i-\bar{x})^3 \tag{17}$$

where $\bar{x}$ is the mean, and σ is the standard deviation of the energy values. The skewness for a normal distribution is zero, in fact any symmetric data will have a skewness of zero. Negative values of skewness indicate that the data are skewed left, while positive values indicate data that are skewed right. Skewed left indicates that the left tail is long relative to the right tail, while skewed right indicates the opposite. For noise only (or very low SNRs), and sufficiently large F, $S \approx 0$. As the SNR increases, S tends to increase.

In [6], exponential functions were fit to the skewness results for T_b = 1 ns and T_b = 4 ns, with S as the x-

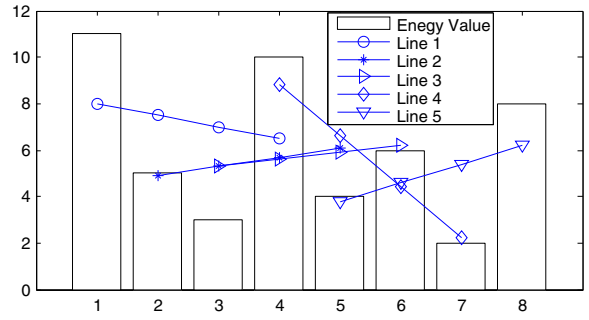

Figure 3 Energy values divided into groups to calculate the slope of each group.

coordinate and ξ_{best} as the y-coordinate. The resulting functions are

$$\xi_{best}^{(1ns)} = 0.9028\text{e}^{-0.1347S} \tag{18}$$

$$\xi_{best}^{(4ns)} = 0.9265\text{e}^{-0.2025S} \tag{19}$$

Maximum slope

Kurtosis and skewness cannot account for delay or propagation time, so the slope of the energy values is considered as an alternative measure. These values are divided into (N_b - M_b + 1) groups, with M_b values in each group. The slope for each group is calculated using a least squares line fit. The maximum slope (M) can then be expressed as

$$M = \max_{1\le n\le N_b - M_b + 1} \text{slope } \{\text{linefit}(z[n], z[n+1], \ldots, \cdot z[n+M_b-1])\} \tag{20}$$

For example, Figure 3 shows the fitted lines for eight energy values and M_b = 4, so there are 8-4 + 1 = 5 lines with 5 corresponding slopes.

Standard deviation

The standard deviation is a widely used measure of variability. It shows how much variation or "dispersion" there is from the average (mean or expected value). The standard deviation is given by

$$\sigma = \sqrt{\frac{\sum_{i=1}^{N_b} (x_i - \bar{x})^2}{N_b - 1}} \tag{21}$$

Joint metric

In order to examine the characteristics of the four statistical parameters (skewness, maximum slope, kurtosis, and standard deviation), the CM1 (residential LOS) and CM2 (residential NLOS) channel models from the IEEE802.15.4a standard are employed. For each SNR value, 1,000 channel realizations were generated and sampled at F_c = 8 GHz. A second derivative Gaussian pulse is employed with T_f = 200 ns, T_c = 1 ns, T_b = 4 ns, and N_s = 1. Each realization has a TOA uniformly distributed within (0, T_f).

The four statistical parameters were calculated, and the results obtained are given in Figures 4 and 5. These figures show that the characteristics of the four parameters with respect to the SNR are similar for the two channels. Further, Figures 4 and 5 show that the kurtosis and skewness increase as the SNR increases, but the skewness changes more rapidly. Conversely, the maximum slope and standard deviation decrease as the SNR increases, but the maximum slope changes more rapidly. Since the skewness and maximum slope change more rapidly than the kurtosis and standard deviation, they better reflect changes in SNR. Therefore, they are more suitable for TOA estimation. Moreover, when the SNR is less than

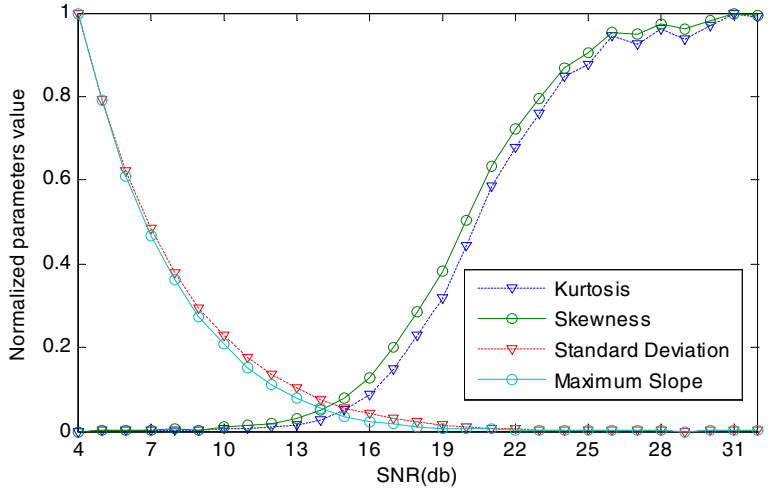

Figure 4 Values of four normalized statistical parameters in channel CM1.

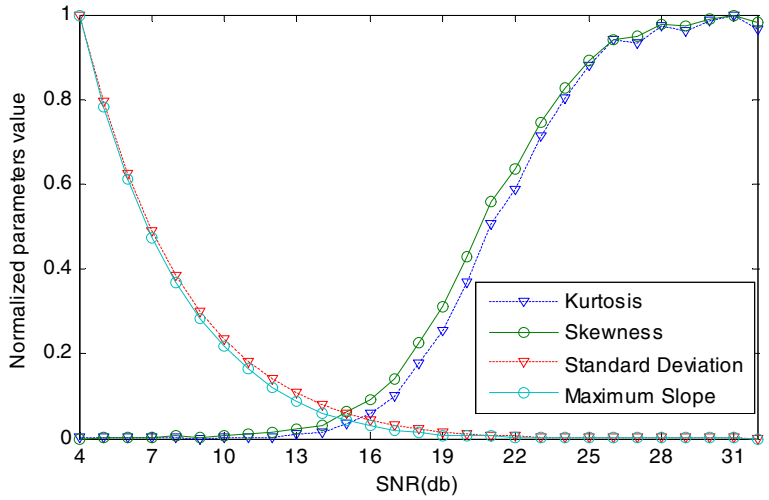

Figure 5 Values of four normalized statistical parameters in channel CM2.

15dB, skewness changes slowly while the maximum slope changes rapidly. On the other hand, when the SNR is higher than 15dB, the skewness changes rapidly but the maximum slope changes slowly. Therefore, no single parameter is a good measure of SNR change over a wide range of values. Thus, the following joint metric based on skewness and maximum slope is proposed.

$$J = S - M, \tag{22}$$

where S is the skewness and M is the maximum slope.

Table 1 shows the standard deviation of the statistics. In all cases, the standard deviations of Maximum Slope and Standard Deviation are much less than 0 and the standard deviations of Skewness and Kurtness increase with the increase of SNRs but the former is much lower than the latter. Therefore, the less variability of Skewness and Maximum Slope implies more confidence about the statistic.

In order to verify that the proposed metric J is sensitive to both high and low SNRs, 1,000 channel realizations were generated for many SNR values in each IEEE802.15.4a channel. In the simulations, because of the random signal, the J values are not unique for one SNR, but in order to draw Figure 6, the average J value with respect to SNR were calculated for each channel model and integration period. Because there were 29 SNR values simulated, there are 29 *J-SNR* pairs for each channel model and integration period. Figure 6 shows that J is a monotonic function for a large range of SNR values, and that J is more sensitive to the changes in SNR than any single parameter. The four curves differ somewhat due to the channel model and integration period used. The figure shows that the metric is more sensitive to T_b than the channel model.

Optimal normalized threshold with respect to *J*

Before training the ANN, the relationship between J and the optimal normalized threshold ξ_{opt} must be established. According to Figure 6, the curves for channel models CM1 and CM2 for a given value of T_b are similar, so models are derived only for T_b=1 ns and T_b=4 ns. There are four steps to establish the relationship between J and ξ_{opt}.

(1) Generate a large number of channel realizations for each channel model, integration period, and SNR value in the range [4, 32] dB.

Table 1 Standard Deviation of the Statistics

SNR	Skewness	Kurtness	Maximum Slope (10E-7)	Standard Deviation (10E-15)
4	0.30	0.92	4.90	1.16
6	0.31	0.95	3.02	0.72
8	0.31	0.93	1.83	0.46
10	0.32	0.97	1.25	0.29
12	0.35	1.22	0.85	0.19
14	0.46	2.23	0.65	0.13
16	0.73	4.36	0.62	0.10
18	1.09	7.82	0.60	0.09
20	1.39	12.04	0.62	0.10
22	1.39	13.46	0.58	0.09
24	1.41	15.11	0.58	0.10
26	1.36	15.20	0.57	0.09
28	1.36	15.73	0.56	0.09
30	1.34	15.65	0.56	0.09
32	1.34	15.76	0.56	0.09

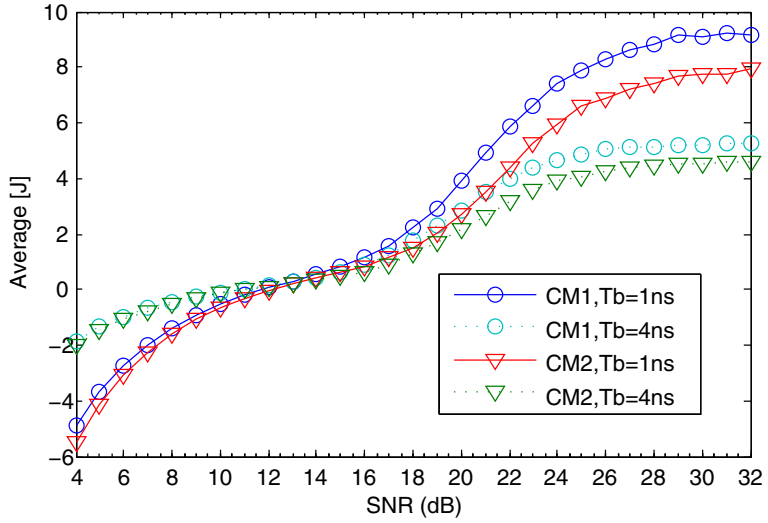

Figure 6 Average *J* values with respect to SNR for different channel models and integration periods.

(2) Calculate the average MAE value with respect to normalized threshold ξ_{norm} for each *J* value, channel model, and integration period as shown in Section "Average MAE with respect to the normalized threshold". In the simulation, because of the random signal, there are many MAE values with respect to one normalized threshold, so the average MAE should be calculated. At the same time, because *J* is a real value, *J* should be rounded to the nearest discrete value, for example integer value or half-integer value.

(3) Select the normalized threshold with the lowest MAE as the best threshold ξ_{best} with respect to *J*

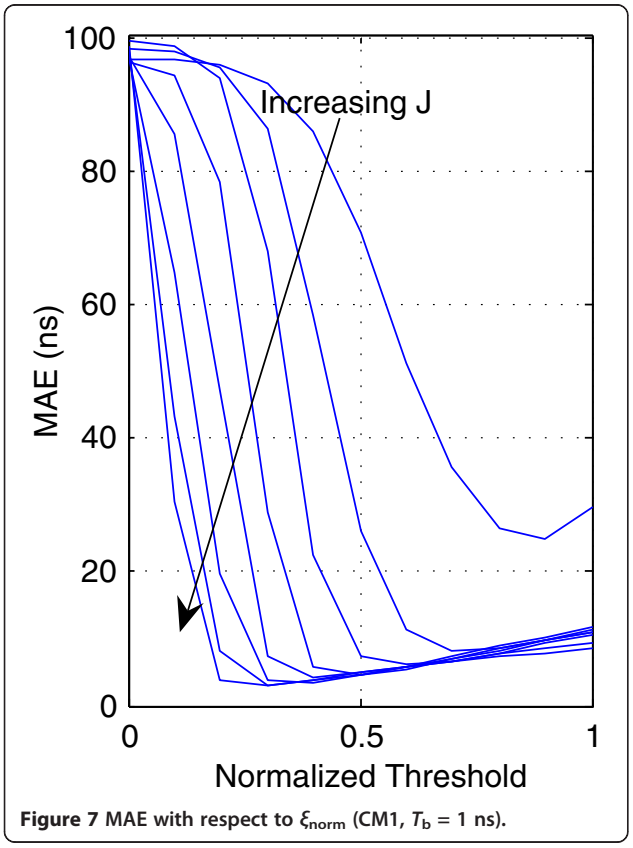

Figure 7 MAE with respect to ξ_{norm} (CM1, T_b = 1 ns).

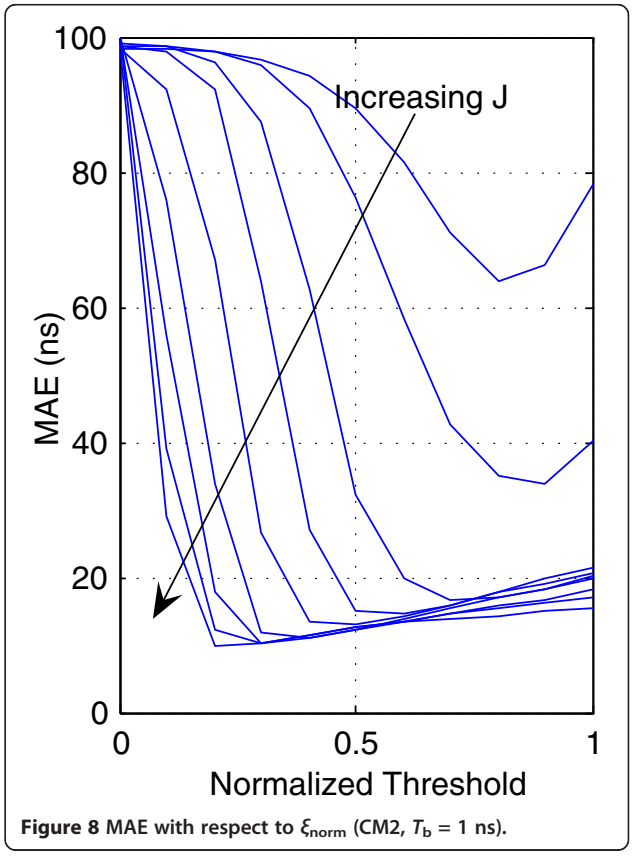

Figure 8 MAE with respect to ξ_{norm} (CM2, T_b = 1 ns).

for each channel model and integration period, as shown in Section "Optimal thresholds".

(4) Calculate the average normalized thresholds of channels CM1 and CM2 for each J as the optimal normalized threshold ξ_{opt}, as shown in Section "Optimal thresholds".

Average MAE with respect to the normalized threshold

To determine the optimal threshold ξ_{opt} based on J, the relationship between the average MAE and the normalized threshold ξ_{norm} for different J, channel model and T_b was determined. ξ is the threshold which is compared to the energy values to find the first TC, as defined (12). When ξ is larger than the maximum energy value z_{max}, no value is found for τ, so in this case ξ is set to z_{max}, and ξ_{norm} is set to 1.

In the simulation, all J values were rounded to the nearest integer and half-integer values for all SNR values, that is, the range [−9, 16] and [−4, 8] for T_b =1 ns and T_b =4 ns. Figures 7, 8, 9 and 10 only show the MAE for integer J = 1 to 8 for the CM1 and CM2 channels, and T_b = 1 ns and T_b = 4 ns. The relationship is always that the MAE decreases as J increases. In addition, the minimum MAE is lower as J increases.

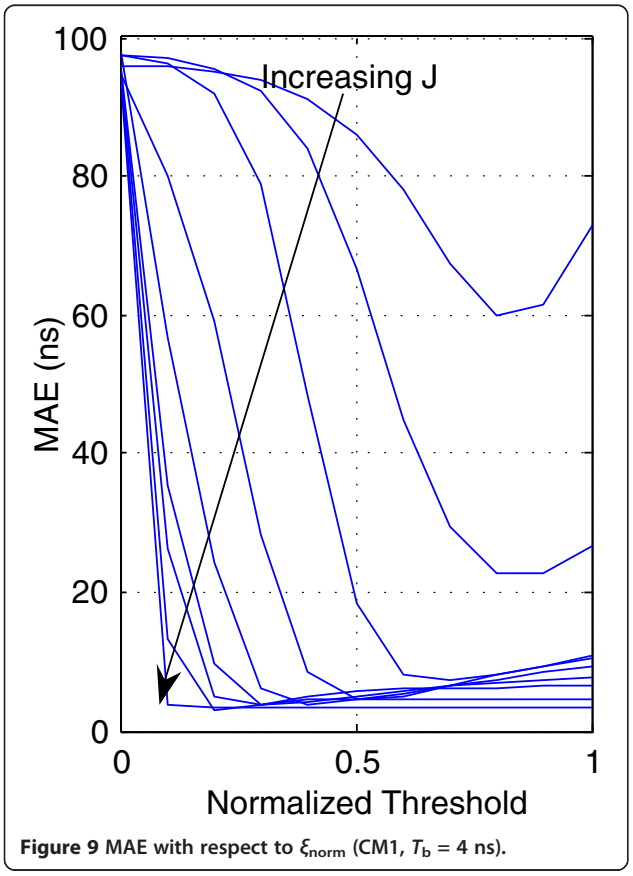

Figure 9 MAE with respect to ξ_{norm} (CM1, T_b = 4 ns).

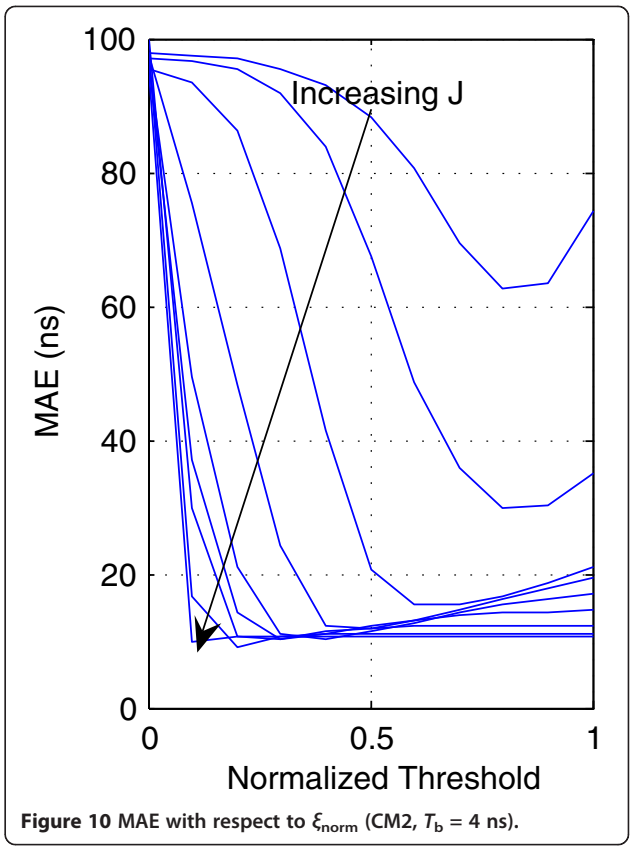

Figure 10 MAE with respect to ξ_{norm} (CM2, T_b = 4 ns).

Optimal thresholds

The normalized threshold ξ_{norm} with respect to the minimum MAE is called the best threshold ξ_{best} for a given J. Therefore, the lowest points of the curves in Figures 7, 8, 9, and 10 for each J are selected as the ξ_{best}. These best thresholds are given in Figures 11 and 12.

These results show that the relationship between the two parameters is not affected significantly by the channel model, but is more dependent on the integration period, so the values for channels CM1 and CM2 can be combined. Therefore, the average of the two values is used as the optimal normalized threshold

$$\xi_{opt}^{(Tb=1ns)}(J) = \frac{\xi_{best}^{(CM1,Tb=1ns)}(J) + \xi_{best}^{(CM2,Tb=1ns)}(J)}{2} \quad (23)$$

$$\xi_{opt}^{(Tb=4ns)}(J) = \frac{\xi_{best}^{(CM1,Tb=4ns)}(J) + \xi_{best}^{(CM2,Tb=4ns)}(J)}{2} \quad (24)$$

Threshold selection using an ANN based on skewness and maximum slope

Structure of the ANN

A BP NN is used which consists of an input layer, a hidden layer and an output layer, as shown in Figure 13.

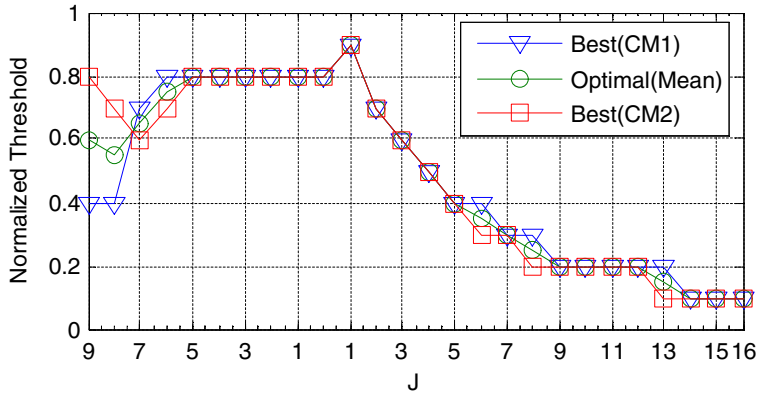

Figure 11 Normalized thresholds with respect to J for T_b = 1 ns.

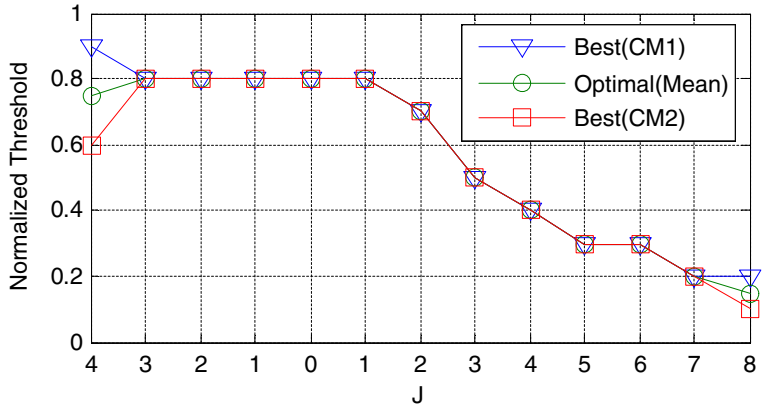

Figure 12 Normalized thresholds with respect to J for T_b = 4 ns.

The weights between the layers are adjusted according to the output layer error.

The number of neurons in the hidden layer is difficult to choose [10], but it can be estimated based on repeated training results. In [11], several ANNs are initialized and trained and the best one is selected. Moreover, in [11], an algorithm (implemented in Matlab) for initializing the ANN weights and biases is used, which warrants the stability and convergence at the beginning of the training. Here, the number of neurons in the hidden layer is varied from 2 to 40, and for each value, the ANN was trained 200 times and the mean squared error (MSE) calculated. The percentage of the MSE values which were less than 1e−10 is given in Figure 14. This shows that as the number of neurons in the hidden layer increases, the percentage also increases, so the effectiveness of the model improves. However, the computational complexity also increases. For T_b = 1 ns, when the number of neurons in the hidden layer is more than 20, the percentage is greater than 90% and changes only slightly with increasing values, so 20 is selected as the number of neurons in the proposed ANN. For T_b = 4 ns, when this number of neurons is more than 10, the percentage is greater than 95% and changes very little with increasing values, so 10 is selected in this case.

The value of ξ_{norm} ranges from 0 to 1, so the logsig function is selected as the transfer function for the neurons of both the hidden and output layers. This function

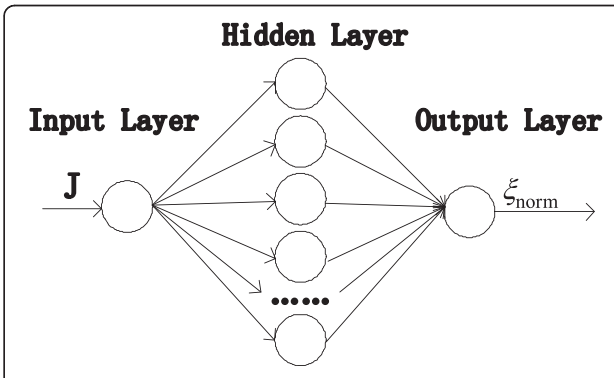

Figure 13 The structure of the ANN.

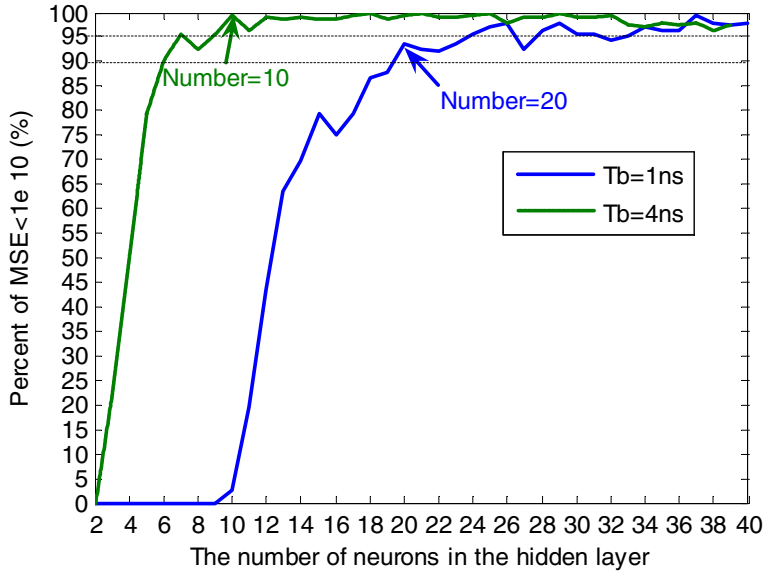

Figure 14 Percentage of the MAE values <1e-10 for a given number of neurons in the hidden layer.

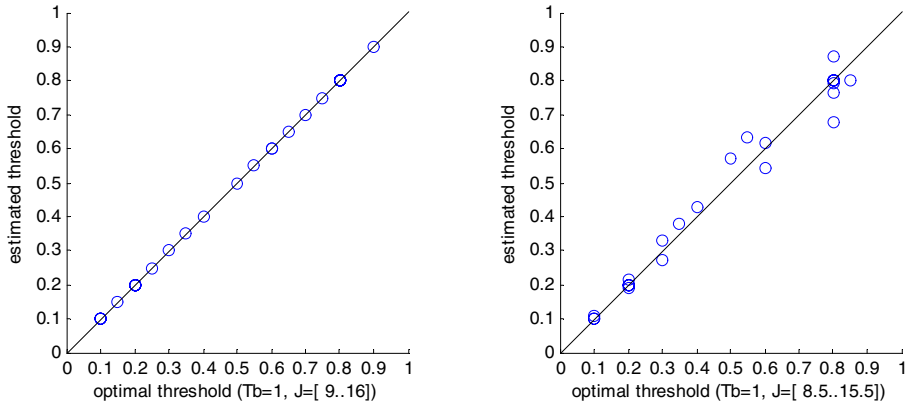

(a) Internal validation for T_b=1ns and J=[9..16] (b) External validation for T_b=1ns and J=[8.5..15.5]

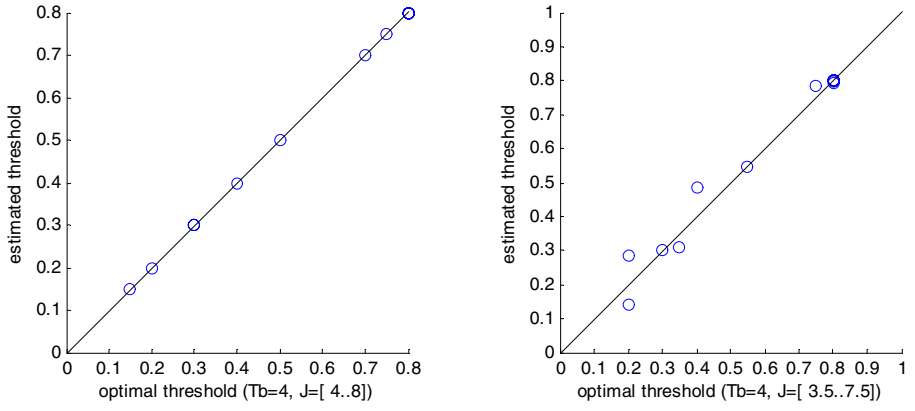

(c) Internal validation for T_b=1ns and J=[9..16] (d) External validation for T_b=1ns and J=[8.5..15.5]

Figure 15 Validation results of the ANN.

Table 2 Validation Results of the ANN

Validation	T_b (ns)	Input of ANN (J)	Coefficient of Determination
Internal	T_b =1	[-9, -8, .., 15, 16]	1
External	T_b =1	[-8.5, -7.5, .. , 14.5, 15.5]	0.9774
Internal	T_b =4	[-4, -3, .. , 7, 8]	1
External	T_b =4	[-3.5, -2.5, .. , 6.5, 7.5]	0.9727

is defind as logsig(x) = 1/(1 + exp(−x)). The Levenberg-Marquardt (LM) algorithm is used in the network training to update the weight and bias values according to LM optimization [12]. Although this algorithm requires more memory than other algorithms, it is often the fastest BP algorithm. Because there is only one input and one output element in the proposed ANN, and only 39 ξ_{norm}-J pairs (J = −9 to 16 for T_b =1 ns and J = −4 to 8 for T_b =4 ns), the memory requirements are modest. The weight and bias values before training were set to random values uniformly distributed between −1 and 1.

ANN training

In order to train the ANN, i.e., to determine the relationship between J and the normalized threshold ξ_{norm}, 1,000 CM1 and CM2 channel realizations for each value of SNR from 4 to 32 dB were generated for both T_b = 1 ns and T_b = 4 ns. The integer J values in the range [−9, 16] and [−4, 8] for T_b =1 ns and T_b =4 ns, respectively, were used to train the ANN. Thus, there were 39 samples to train the ANN. On the other hand, the half-integer J values in the range [−0.85, 15.5] and [−3.5, 7.5] for T_b =1 ns and T_b =4 ns, respectively, were used to conduct the external validation for the trained ANN. To obtain the best ANN, 100 separate training iterations were conducted for each value of T_b, and the one with the lowest MSE was selected.

Validation of the ANN

In order to evaluate the performance of the trained ANN, the internal validation and the external validation were both conducted as shown in Table 1 and Figure 15. The J values from −9 to 16 for the internal validation with T_b =1 ns, from −8.5 to 15.5 for the external validation with T_b =1 ns, from −4 to 8 for the internal validation with T_b =4 ns and from −3.5 to 7.5 for the external validation with T_b =4 ns were input to the ANN to get the estimated normalized thresholds. As shown in Table 2, the two coefficients of determination of the internal validation for T_b =1 ns and T_b =4 ns are both nearly equal to 1 and the two coefficients of determination of the external validation for T_b =1 ns and T_b =4 ns are both more than 0.97, so the trained ANN output fits well with the optimal normalized thresholds for T_b =1 ns and T_b =4 ns. However, the ANN is able to provide values for any J, and not just discrete values. The ANN also eliminates the complicated and time-consuming optimization process used in Section "Optimal normalized threshold with respect to J". The IEEE802.15.4a channel models reflect the statistical properties in specific environments, and the choice of ANN parameters depends on the characteristics of the channel. Our ANN can easily be employed with any channel, and the parameters adjusted to fit any environment. This is particularly useful when the channel is not static.

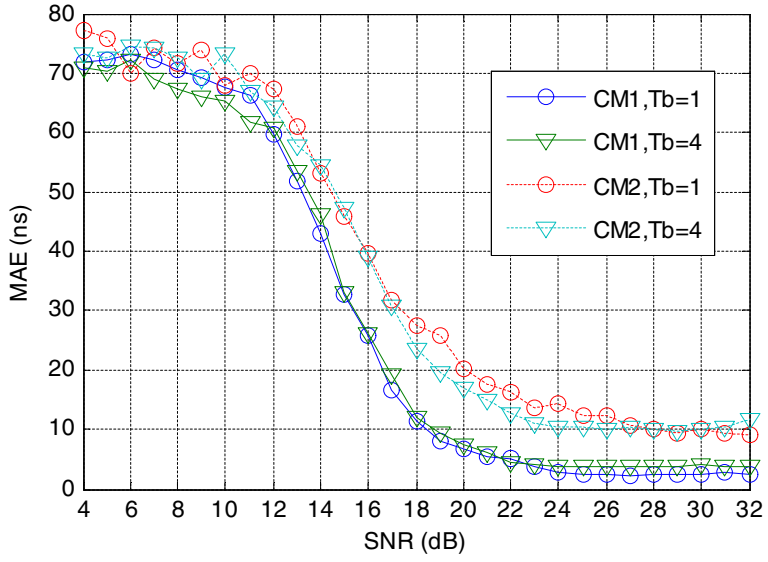

Figure 16 MSE for channels CM1 and CM2 with T_b = 1 ns and 4 ns.

Table 3 MAE averaged over all the simulated realizations

Channel model	T_b	MAE (ns)			
		ANN	Fixed-Threshold	MES	Kurtosis
CM1	1 ns	29.54	50.48	38.09	42.74
	4 ns	29.66	50.13	38.93	63.57
CM2	1 ns	37.88	58.51	47.12	50.12
	4 ns	36.64	57.03	46.00	69.20

Performance results and discussion

In this section, the MAE is examined for different ED based TOA estimation algorithms in the IEEE 802.15.4a channel model CM1 and CM2. As before, 1,000 channel realizations were generated for each case. A second derivative Gaussian pulse with a 1 ns pulse width was employed, and the received signal sampled at F_c = 8 Ghz. The other system parameters were T_f = 200 ns and N_s =1. Each realization had a TOA uniformly distributed within (0, T_f).

Figure 16 presents MAE of the TOA estimation based on the ANN for SNR values from 4 to 32 dB in the LOS (CM1) and NLOS (CM2) channels with T_b = 1 ns and 4 ns. This shows that the ANN algorithm performs well at high SNRs. The performance in CM1 is better than in CM2 by at most 18 ns. When SNR > 22 dB, the MAE for CM1 is less than 3.85 ns while for CM2 it is less than 11 ns. In most cases, the performance with T_b = 1 ns is better than that with T_b = 4 ns, regardless of the channel, but the difference is less than 4 ns.

Table 3 shows the MAE averaged over all the simulated realizations. Here "ANN" refers to the proposed algorithm, "MES" to the MES algorithm, and the normalized threshold for the FT algorithm is set to 0.4. In all cases, the average MAE of ANN is the lowest among the four algorithms.

Figures 17 and 18 present the MAE for four TOA algorithms in channels CM1 and CM2, respectively. As expected based on the results in Section "Statistical characteristics of the signal energy", the MAE with the proposed algorithm is lower than with the other algorithms, particularly at low to moderate SNR values. The proposed algorithm is better than the Kurtosis algorithm except when the SNR is greater than 27 dB. For these large SNR values, the Kurtosis algorithm is slightly better. For example, when SNR > 27 dB, the MAE of the proposed ANN algorithm is at most 2 ns greater than that of the Kurtosis algorithm.

The performance of the proposed algorithm is more robust than the other algorithms, as the difference between T_b = 1 ns and 4 ns is very small compared to the difference with the Kurtosis algorithm. For almost all SNR values the proposed algorithm is the best. Conversely, the performance of the Kurtosis algorithm varies greatly with respect to the other algorithms, and is very poor for low to moderate SNR values.

Conclusions

A low complexity ANN-based (TOA) estimation algorithm has been developed for UWB remote sensing applications. Four statistical parameters were investigated, and from the results obtained, a joint metric based on skewness and maximum slope was developed for TC TOA estimation. The optimal normalized threshold was determined using performance results for the CM1 and CM2 channels. The effects of the integration period and channel model were investigated. It was determined that the proposed threshold selection technique is largely independent of the channel model. The performance of the proposed algorithm is shown to be better than several well-known algorithms. In addition,

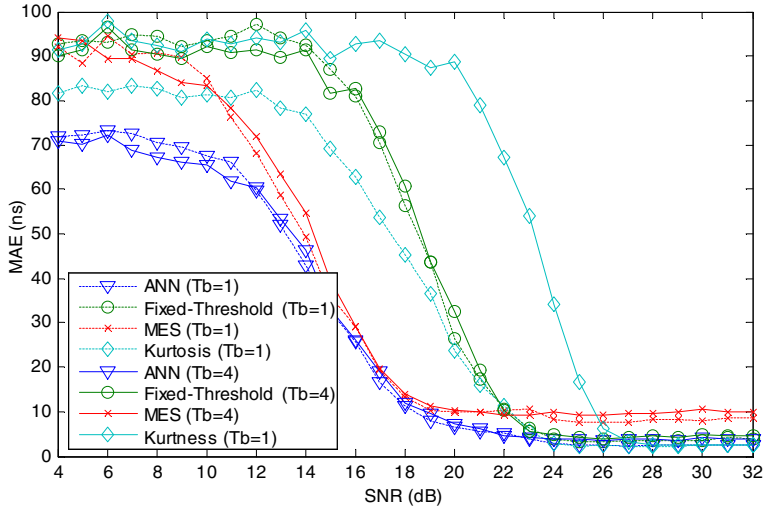

Figure 17 MAE for different algorithms with channel CM1.

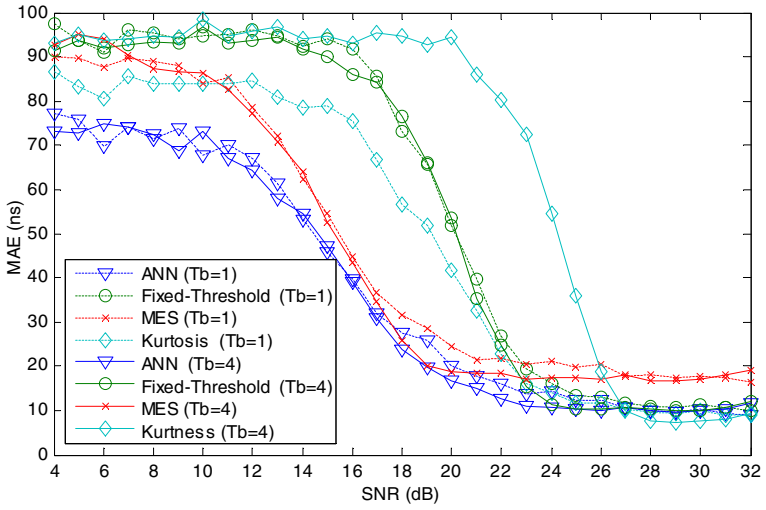

Figure 18 MAE for different algorithms with channel CM2.

the proposed algorithm is more robust to changes in the SNR and integration period.

Competing interests

The authors declare that they have no competing interests.

Acknowledgments

This study was supported by the Nature Science Foundation of China under grant No. 60902005, the Outstanding Youth Foundation of Shandong Province under grant No. JQ200821, and the Program for New Century Excellent Talents of the Ministry of Education under grant No. NCET-08-0504.

Author details

[1]Department of Information Science and Engineering, Ocean University of China, Qing Dao, China. [2]Department of Computer and Communication Engineering, China University of Petroleum (East Chinxa), Qing Dao, China. [3]Department of Electrical Computer Engineering, University of Victoria, Victoria, Canada.

Received: 12 July 2011 Accepted: 2 August 2012
Published: 25 August 2012

References

1. S. Foo, A. Walsh, S. Kashyap, *Ultra-wideband (UWB) remote sensing and radar imaging* (, 2004). http://pubs.drdc.gc.ca /PDFS/unc36/p521851.pdf. Accessed 23 Feb 2011
2. L. Talbi, Y. Rissafi, A. Lakhssassi, UWB measurement investigation for remote sensing in underground mining environment. In Proceedings of the International Conference on Electromagnetics in Advanced Applications **11**, 1030–1033 (2009). doi:10.1109/ICEAA.2009.5297778. Torino, Italy, 14-18 September
3. A.Y.-Z. Xu, E.K.S. Au, A.K.-S. Wong, Q. Wang, A novel threshold-based coherent TOA estimation for IR-UWB systems. IEEE Trans. Vehic. Technol **58**, 4675–4681 (2009). doi:10.1109/TVT.2009.2020990
4. I. Guvenc, Z. Sahinoglu, Threshold selection for UWB TOA estimation based on kurtosis analysis. IEEE Commun. Letters **9**, 1025–1027 (2005). 10.1109/LCOMM.2005.1576576
5. I. Guvenc, Z. Sahinoglu, Threshold-based TOA estimation for impulse radio UWB systems. Proceedings of the IEEE International Conference on Ultra-wideband, Zurich **2005**, 420–425 (2005). doi:10.1109/ICU.2005.1570024. 5–8 September
6. H. Zhang, X.-R. Cui, T.A. Gulliver, Threshold selection for ultra-wideband TOA estimation based on skewness analysis. Proceedings of the 8th International Conference on Ubiquitous Intelligence and Computing. Banff, AB **6905 LNCS**, 503–513 (2011). doi:10.1007/978-3-642-23641-9_40. 2–4 September
7. I. Guvenc, Z. Sahinoglu, Multiscale energy products for TOA estimation in IR-UWB systems. Proceedings of the IEEE Global Telecommunications Conference, St. Louis, MO **1**, 209–213 (2005). doi:10.1109/GLOCOM.2005.1577382. 28 November - 2 December
8. A.F. Molisch, K. Balakrishnan, D. Cassioli, C.-C. Chong, S. Emanmi, A. Fort, F. Karedal, J. Kunisch, H. Schantz, U. Schuster, K. Siwiak, *IEEE 802.15.4a Channel Model—Final Report* (, 2006). IEEE P802.15-04-0662-00-004a
9. H. Zhang, T.A. Gulliver, Capacity of time-hopping PPM and PAM UWB multiple access communications over indoor fading channels. Eurasip J. Wireless Commun. and Networking **2008**, 1–9 (2008). doi:10.1155/2008/273018
10. S. Haykin, *Neural Networks: A Comprehensive Foundation*, 2nd edn. (Prentice-Hall, London, 1999)
11. R. Vicen-Bueno, R. Carrasco-Alvarez, M. Rosa-Zurera, J.C. Nieto-Borge, M.P. Jarabo-Amores, Artificial neural network-based clutter reduction systems for ship size estimation in maritime radars. EURASIP J. Advances in Signal Processing **2010**, 1–15 (2010). 10.1155/2010/380473
12. G. Lera, M. Pinzolas, Neighborhood based Levenberg-Marquardt algorithm for neural network training, IEEE Trans. Neural Networks **13**, 1200–1203 (2002). 10.1109/TNN.2002.1031951

doi:10.1186/1687-6180-2012-185
Cite this article as: Zhang *et al.*: Remotely-sensed TOA interpretation of synthetic UWB based on neural networks. *EURASIP Journal on Advances in Signal Processing* 2012 **2012**:185.